◆ Human Brain Mapping 6:283–300(1998) ◆

# Modeling Hemodynamic Response for Analysis of Functional MRI Time-Series

**Jagath C. Rajapakse,[1]* Frithjof Kruggel,[1] Jose M. Maisog,[2] and D. Yves von Cramon[1]**

[1]*Max-Planck-Institute of Cognitive Neuroscience, Leipzig, Germany*
[2]*Section on Functional Brain Imaging, Laboratory of Psychology and Psychopathology, National Institute of Mental Health, Bethesda, Maryland*

**Abstract:** The standard Gaussian function is proposed for the hemodynamic modulation function (HDMF) of functional magnetic resonance imaging (fMRI) time-series. Unlike previously proposed parametric models, the Gaussian model accounts independently for the delay and dispersion of the hemodynamic responses and provides a more flexible and mathematically convenient model. A suboptimal noniterative scheme to estimate the hemodynamic parameters is presented. The ability of the Gaussian function to represent the HDMF of brain activation is compared with Poisson and Gamma models. The proposed model seems valid because the lag and dispersion values of hemodynamic responses rendered by the Gaussian model are in the ranges of their previously reported values in recent optical and fMR imaging studies.

An extension of multiple regression analysis to incorporate the HDMF is presented. The detected activity patterns exhibit improvements with hemodynamic correction. The proposed model and efficient parameter estimation scheme facilitated the investigation of variability of hemodynamic parameters of human brain activation. The hemodynamic parameters estimated over different brain regions and across different stimuli showed significant differences. Measurement of hemodynamic parameters over the brain during sensory or cognitive stimulation may reveal vital information on physiological events accompanying neuronal activation and functional variability of the human brain, and should lead to the investigation of more accurate and complex models. *Hum. Brain Mapping 6:283–300, 1998.* 

**Key words:** brain imaging; blood-oxygen-level-dependent contrast; functional magnetic resonance imaging; hemodynamic response function; multiple regression

## INTRODUCTION

Functional magnetic resonance imaging (fMRI) methods have been successfully employed to localize dynamic brain processes in various stimulation tasks [Bandettini et al., 1993, 1994; Belliveau et al., 1991; Blamire et al., 1992; Engel et al., 1994; Kwong et al., 1992; McCarthy et al., 1993; Turner et al., 1993]. The most popular of these methods exploit the differences in the magnetic susceptibilities of oxygenated hemoglobin ($HbO_2$) and deoxygenated hemoglobin (HbR) to track the blood-flow-related phenomena of neuronal activations, which is referred to as blood-oxygen-level-dependent (BOLD) contrast [Bandettini et al., 1994; Duyn et al., 1994; Menon et al., 1993, 1995; Ogawa et al., 1992, 1993]. HbR concentration changes concomitant with synaptic activities modulate local micro-

*Correspondence to: Jagath C. Rajapakse, Ph.D., Max-Planck-Institute of Cognitive Neuroscience, Inselstrasse 22–26, D-04103 Leipzig, Germany. E-mail: raja@cns.mpg.de

Received for publication 19 March 1997; accepted 7 April 1998

scopic $B_0$ field gradients in the vicinity of blood cells and veins [Bandettini et al., 1994], altering the signal intensities of $T_2$- and $T_2^*$-weighted MR sequences.

There are still controversies as to the vascular and tissue origin of the fMRI intensity changes observed at various field strengths. A transient shortening of $T_2^*$ within milliseconds after the onset of stimulus, which is attributed to the rapid increase in $O_2$ consumption upon onset of neural firing, has been reported [Ernst and Henning, 1994; Menon et al., 1994]. This is followed by an increase of fMRI signal due to slower hemodynamic response, which overcompensates the initial hypooxygenation and oversupplies the active region, leading to an increase in $HbO_2$ concentration with respect to the baseline value. In vivo optical imaging of intrinsic signals [Frostig et al., 1990] revealed a transient increase of blood flow within the first 1,000 msec of neuronal activity, and recent MR imaging experiments demonstrated a maximal rise in oxyhemoglobin, 5–8 sec after the onset of neuronal activity [Bandettini et al., 1993; Lee et al., 1995]. The above observations evince that the hemodynamic responses due to synaptic activities are delayed and dispersed in time, and transient at the onset and offset of the stimulus condition.

Our interpretation and application of fMRI techniques are based on the observation that the BOLD effect correlates with local energy consumption, which in turn correlates with neuronal firing [Raichle et al., 1976; Fox and Raiche, 1986; Fox et al., 1988; Jueptner and Weiller, 1995]. The mechanism of coupling of neuronal activations to the vascular system is still unknown and produces significant blurring and delay to the original neuronal responses over time, indicating a low-pass filtering operation. Hemodynamic events have time scales of a few seconds, whereas neuronal events have time constants of milliseconds. Without knowing the proper mechanism of coupling between neuronal responses and hemodynamics, exact modeling of the complex function of vascular coupling is currently impossible.

Recent linear convolution models where vascular coupling is considered as a functional convolution provide a reasonable approximation [Friston et al., 1994; Villringer and Dirnagl, 1995; Lange and Zeger, 1997; Cohen, 1997]. Following this linear approach, we will investigate the standard Gaussian function [Maisog et al., 1995] as the point spread function of vascular coupling of neuronal activations or the *hemodynamic modulating function* (HDMF). HDMFs are characterized by two parameters, namely *lag* and *dispersion*, where lag represents the time delay between the hemodynamic response and ensuing neural activations, and dispersion represents the temporal smoothness or autocorrelation of hemodynamic response. The Poisson function was the first to be proposed as the HDMF of the brain [Friston et al., 1994], and the first to render global values of lag and dispersion of 7.67 sec in a visual stimulation experiment. A disadvantage of the Poisson HDMF is its discrete nature and the representation of delay and dispersion with a single parameter. The Gamma function has been proposed recently [Lange and Zeger, 1997; Cohen, 1997]; however, the lag and dispersion provided by the Gamma function are not independent (see Appendix). Another major obstacle for the practical use of the Gamma model is the need for nonlinear iterative optimization schemes to estimate its parameters. Though the data-driven nonparametric approaches have shown their capabilities to handle transients, the Gamma function has been superior in modeling lag and dispersion aspects of hemodynamic responses [Nielsen et al., 1997]. In what follows, our focus will be restricted only to parametric models of HDMF.

The primary aim of this paper was to introduce the standard Gaussian model as a more natural, flexible, and mathematically tractable HDMF, especially when a space-variant and stimulation-dependent approach is taken. The Gaussian model is validated by comparing the lag and dispersion values reported in the optical intrinsic imaging literature and recent fMRI experiments. The ability of the Gaussian model to represent HDMF of human brain activation will be compared with Poisson and Gamma models. In fact, at large lag and dispersion values, both Poisson and Gamma models approximate the Gaussian model. It will be shown how knowledge of the HDMF is utilized to improve the analysis of fMRI data with univariate multiple regression analysis.

Frequency-domain observations of fMRI time-series in the motor cortex [Bandettini et al., 1993] and occipital cortex [Bullmore et al., 1996] have demonstrated peak neural activities at the first and second harmonics of the fundamental frequency of the stimulus conditions. Here we utilize all sufficiently powerful harmonics of the frequency of the time-series to devise a suboptimal and noniterative scheme to estimate the hemodynamic parameters. This scheme provides an efficient and fast method of evaluating hemodynamic parameters at every brain voxel, facilitating the investigation of their variability over different brain regions and different stimuli. Previously, the same parameters were used for hemodynamic responses over the entire brain and for all types of stimulations [Friston et al., 1994b; Worsley and Friston, 1995], mainly because of the lack of an efficient and pragmatic scheme to

evaluate these parameters at every brain voxel. The fMRI experiments with visual-stimulation, word-discrimination, and sentence-processing tasks demonstrate the need for a space-variant and stimulation-dependent model for the HDMF of the brain. Knowledge of the hemodynamic parameters at a brain site may provide vital information on local metabolic events, synaptic activities, and blood flow ensuing upon neuronal activation. For instance, the different delays in hemodynamic responses have been used to distinguish veins and capillaries in activated tissue areas and beyond [Singh et al., 1995; Lee et al., 1995].

The idea of the HDMF is phenomenological and provides an approximation and approach to investigate vascular coupling of brain activation and associated neuronal events. A candidate for HDMF should have enough degrees of freedom to fit the actual hemodynamic response, and its parameters should highlight salient aspects of related biological events. We favor the Gaussian model because of its two degrees of freedom to independently represent lag and dispersion and its mathematical convenience. The reason reported for the selection of the Gamma family for HDMF was the existence of continuous Fourier transforms of their derivatives [Lange and Zeger, 1997]. However, due to insufficient knowledge of the exact process of hemodynamic coupling and therefore the absence of a gold standard for human brain activation, it is not possible to accurately judge the superiority of a particular model. Nevertheless, these models have the potential to investigate and quantitate hemodynamic and neuronal events in response to sensory and cognitive stimulation [see Rajapakse and Kruggel, 1997].

The organization of this paper is as follows. The next section introduces the Gaussian HDMF to model hemodynamic responses, and is followed by the frequency-domain analysis to estimate its parameters. We then explain the analysis of fMRI time-series and the adjustments necessary for the univariate multiple regression analysis to cope with the spatial and temporal correlations. Results of fMRI experiments follow. Finally, our approach, its limitations, and our results are discussed.

## A MODEL FOR CEREBRAL HEMODYNAMIC RESPONSE

Intensities of fMRI image voxels obtained using a $T_2^*$-weighted sequence in a sensory or cognitive stimulation represent changes in local concentrations of HbR, which are referred to as *hemodynamic responses* at brain voxels. To sustain neuronal firing in response to sensory or cognitive stimuli, metabolic events concur with increased local energy consumption. Due to the finite size of the image voxels, the hemodynamic responses represent the average changes of HbR concentration within the space occupied by the corresponding brain voxels. By *neuronal activity*, we mean the energy consumption within a brain voxel which is physiologically coupled to local hemodynamics. The image resolution in fMRI permits detecting hemodynamic contributions from both capillaries and veins which carry deoxygenated blood in response to some neuronal activity [Fahm et al., 1994].

If the hemodynamic response at a brain site at time t due to neuronal activity v(t) is denoted by w(t), the coupling between the neuronal activity and hemodynamic response of our model is given by

$$w(t) = \gamma v(t) \otimes h(t) + \eta(t) \tag{1}$$

where $\gamma$ denotes the gain of the vascular coupling, h(t) represents the HDMF, and $\eta(t)$ is the noise in the hemodynamic response. The convolution operation denoted by "$\otimes$" is referred to as *hemodynamic modulation*. A unit impulse of neuronal activity produces hemodynamic response equal to the gain $\gamma$. The hemodynamic noise is assumed to be random and $\eta(t) \sim N(0, s_h^2)$ where $s_h^2$ is the variance of the noise.

The major assumptions of our model for fMRI time-series are that 1) the input stimulus pattern appears without distortion as the synaptic input to the brain voxel, and 2) the hemodynamic responses at brain voxels are completely recoded at the fMRI image voxels. That is, if y(t) denotes the time-series signal and x(t) the sensory or cognitive stimulation, we presume $x(t) \propto v(t)$ and $y(t) \propto w(t)$. By substituting these in Eq. (1), we obtain:

$$y(t) = \alpha x(t) \otimes h(t) + \epsilon(t) \tag{2}$$

where $\alpha$ denotes the *gain* of the fMR imaging process and $\epsilon(t)$ represents the noise in the time-series with $\epsilon(t) \sim N(0, s^2)$. The gain $\alpha$ was introduced to separately account for the scaling of signals, and this necessitates the integral of the h(t) over time to be unity:

$$\int_{-\infty}^{\infty} h(t)\, dt = 1. \tag{3}$$

This condition is mandatory for the probability density functions and, in fact, all three parametric models, Poisson, Gamma, and Gaussian, are widely-used density functions in the theory of probability.

Below, we define two parameters, namely, lag and dispersion of a given HDMF h(t):

$$\text{lag} \triangleq \int_{-\infty}^{\infty} \text{th}(t)\, dt \tag{4}$$

$$\text{dispersion} \triangleq \int_{-\infty}^{\infty} (t - \text{lag})^2 h(t)\, dt. \tag{5}$$

The lag and dispersion are the first moment and second central moment of the HDMF, respectively. If the condition in Eq. (3) is not mandatory, these parameters need to be defined as their normalized moments. It can be easily shown that a function, when convolved with h(t), will be delayed with an amount equal to lag and smoothed with a scale equal to the square root of dispersion. In hemodynamic responses, lag represents the delay in the excess blood supply to the activated sites following the onset of neuronal firing, which depends on blood pressure, blood regulation, etc., and dispersion represents the amount of autocorrelation present in the hemodynamic responses, which depends on the differential rates of neuronal firing and blood flow, and the events across the blood-brain barrier. Interestingly, the two parameters of mean and variance of the Gaussian function are equal to the lag and dispersion of the HDMF. Ironically, the lag and dispersion values provided by Poisson and Gamma models are related to each other (see Appendix).

In our model, $h(t) = G(t; \mu, \sigma)$ where:

$$G(t; \mu, \sigma) = \frac{1}{\sqrt{2\pi\sigma^2}} e - (t - \mu)^2 / 2\sigma^2. \tag{6}$$

$\mu$ and $\sigma^2$ are the lag and dispersion, respectively. The space of the HDMFs offered by the Gaussian model is $\{G(t; \mu, \sigma), \mu \epsilon R, \sigma^2 \epsilon R^+\}$, where an element of this functional space produces a Gaussian form of autocorrelation in the neuronal responses. Figure 1 shows the plots of HDMFs of Poisson, Gamma, and Gaussian models and their frequency spectra (the parameters of these plots correspond to the largest activated region in the representative slice in the visual-stimulation experiment shown in Figure 2.

Our model defined by Eqs. (2) and (6) is linear, and the complexity of the convolution operation is conveniently handled by the frequency-domain analysis. By taking the Fourier transform of Eq. (2), one can write:

$$Y(\omega) = \alpha H(\omega) X(\omega) + E(\omega) \tag{7}$$

where $F(\omega)$ represents the Fourier transform of the function f(t). Except for the Poisson function, which does not have an analytical expression for the Fourier transform, the parameters of both Gamma and Gaussian models are estimated using the frequency-domain analysis.

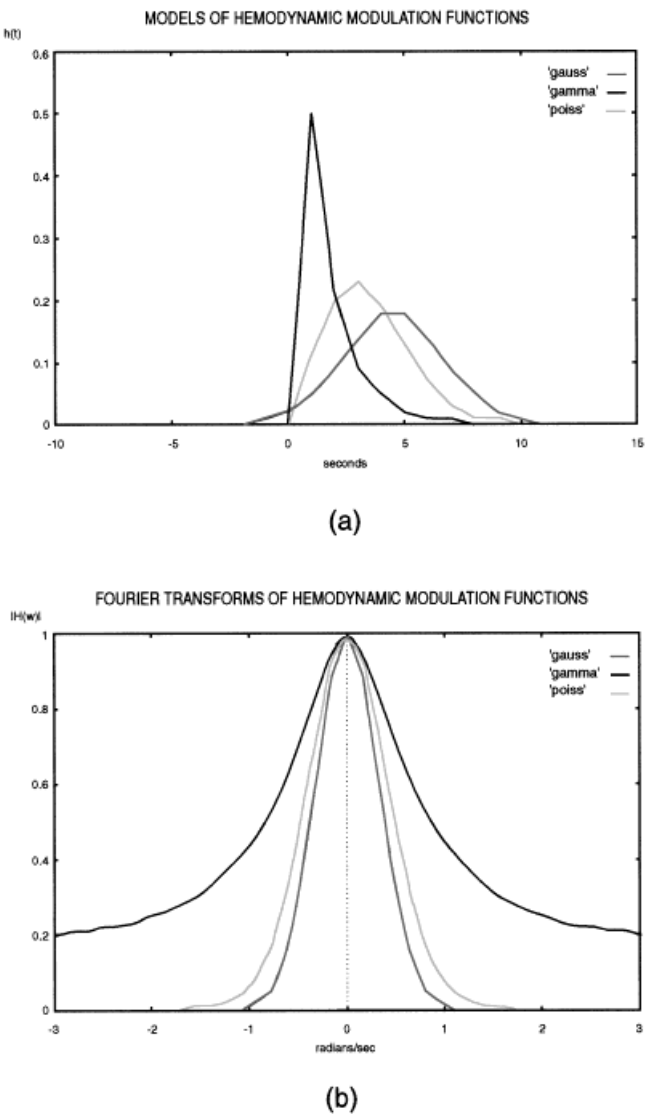


**Figure 1.**
Parametric models of hemodynamic modulation functions (HDMFs) **a:** Time-domain plots. **b:** Their frequency spectra. Parameters for the plots were those obtained from the largest activation region in a representative slice in a visual-stimulation experiment; parameters for Poisson model $\lambda = 3.0$ sec, for Gamma model $\theta_1 = 0.46$ and $\theta_2 = 0.15$, and Gaussian model $\mu = 4.50$ s and $\sigma^2 = 4.721$ s$^2$.

## ESTIMATION OF HEMODYNAMIC PARAMETERS

In the above analysis, the fMRI time-series and stimulus conditions were considered to be continuous-

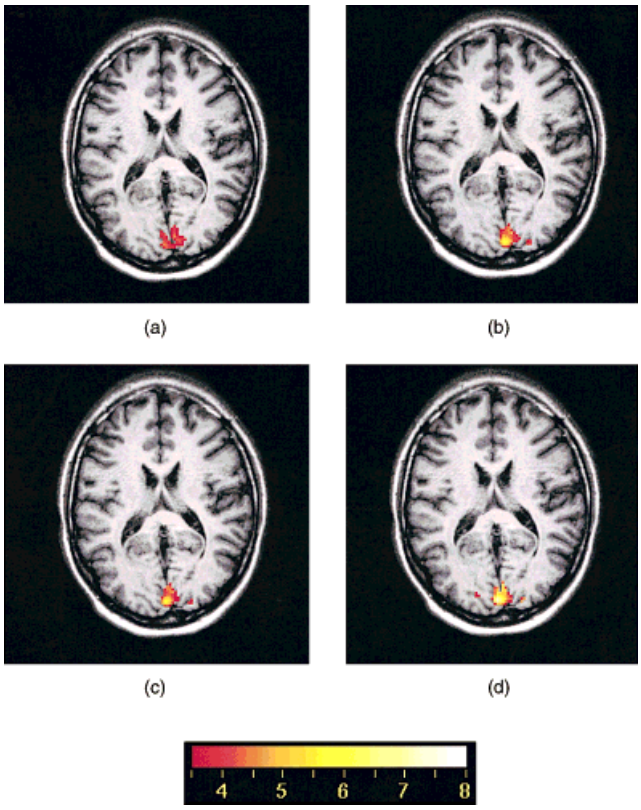


**Figure 2.**
Significant activations on a single axial slice obtained in a visual-stimulation experiment using univariate multiple regression analysis. **a:** Without hemodynamic correction ($z \geq 3.0$). b–d: With hemodynamic correction ($z \geq 3.5$), using (**b**) Poisson, (**c**) Gamma, and (**d**) Gaussian models.

time functions. Although the brain responses are continuous-time functions, the fMRI time-series are discrete-time functions defined over a finite duration of time, and henceforth our analysis will be in discrete-time domain. We suppose that the input sensory and cognitive stimulations are periodic and presented at regular intervals synchronized to the fMRI image scans. Let us denote the scanning interval by $\Delta$ and the ith stimulation sample in the time-series by $y_i$. Then $y_i = y(\Delta i)$ where $i = 1, 2, \ldots, n$. The total number of samples in the time-series, or of scans in the fMRI image, is n. Let us denote the input stimulation by vector $x = (x_1, x_2, \ldots, x_n)^T$, and the time-series output by vector $y = (y_1, y_2, \ldots, y_n)^T$.

Consider an input stimulus having T samples per period with N stimulation cycles. For such a stimulus, the discrete Fourier transform (DFT) corresponding to Eq. (7) is given by

$$Y(\omega_l) = \alpha H(\omega_l)X(\omega_l) + E(\omega_l) \qquad l = 0 \ldots T - 1 \quad (8)$$

where $F(\omega_l) = \Sigma_{i=0}^{T-1} f_T(t)e^{-i\omega_l l}$ and $\omega_l = 2\pi l / T$. $\omega_l$ represents the lth harmonic of the fundamental frequency $\omega_l = 2\pi / T$ of the time-series. The $f_T(t)$ represents the average period of the periodic function f(t) with a period T. Because the experimental design determines $X(\omega_l)$, the set of equations defined by Eq. (8) can be utilized to determine the optimal parameters of the HDMF, h(t). The standard approach is to attempt to find the $\chi^2$-fitting or weighted least-square estimation which minimizes the cost function $\chi^2$ [Press et al., 1994]:

$$\chi^2 = \sum_{t=1}^{T-1} (Y(\omega_l) - \alpha H(\omega_l)X(\omega_l))^*(Y(\omega_l) - \alpha H(\omega_l)X(\omega_l)) / \sigma_l^2 \quad (9)$$

where * denotes the complex conjugate and $\sigma_l^2$ the variance of the noise at the lth harmonic frequency. The above cost function is usually a nonlinear function of hemodynamic parameters, which requires the use of iterative and numerical optimization techniques to determine optimal parameters [Press et al., 1994]. Finding the $\chi^2$-fitting is further complicated by the involvement of the complex quantities in Eq. (9). A major pitfall of this iterative and rigorous approach is the instability caused by attempting to fit the time-series of nonactivated voxels to the model, because the time-series parameters need to be evaluated before the identification of activated and nonactivated voxels. To avoid this problem, we propose a noniterative suboptimal scheme for the parameter estimation of the Gaussian HDMF in the rest of this section.

Neglecting noise $E(\omega_l)$, substituting $H(\omega_l) = e^{-\omega_l^2\sigma^2/2}e - j\omega_l\mu$ [Papoulis, 1991] for the Gaussian HDMF, and equating magnitudes of frequency responses of both sides of Eq. (8), one can obtain:

$$2 \log(\alpha) - \omega_l^2\sigma_l^2 = L_l \quad (10)$$

where $L_l = \log(|Y(\omega_l)|^2 / |X(\omega_l)|^2)$. By equating phase angles of both sides of Eq. (8), one can write:

$$-\mu\omega_l = \phi_l \quad (11)$$

where $\phi_l = \tan^{-1}(Y(\omega_l) / X(\omega_l))$ and $l = 0, 1, \ldots, T - 1$.

For each harmonic frequency $\omega_l$, we have two equations consisting of three parameters in the set $[\alpha, \mu, \sigma^2]$. Because we have a large number of equations to evaluate three parameters, optimal parameters are obtained using the least square estimations of Eqs. (10) and (11). To compensate for the errors and instability caused by our assumption on noise, only the harmon-

ics which have sufficient power in the input stimulus are considered for the least square estimation. If $\Omega$ denotes the set of harmonics which have power above the minimum power P, $\Omega = \{l; |X(\omega_l)|^2 > P, l = 0, 1, \ldots, T-1\}$. Then, the following equations for least-square estimation can be easily obtained:

$$\hat{\alpha} = \exp\{(S_3S_4 - S_5S_2)/2(S_1S_4 - S_2S_2)\} \quad (12)$$

$$\hat{\mu} = S_6/S_2 \quad (13)$$

$$\hat{\sigma}^2 = (S_3S_2 - S_5S_2)/(S_1S_4 - S_2S_2) \quad (14)$$

where $S_1 = \Sigma_{l\epsilon\Omega}$, $S_2 = \Sigma_{l\epsilon\Omega}\,\sigma_l^2$, $S_3 = \Sigma_{l\epsilon\Omega}\,L_l^2$, $S_4 = \Sigma_{l\epsilon\Omega}\,\omega_l^4$, $S_5 = \Sigma_{l\epsilon\Omega}\,L_l\omega_l^2$, and $S_6 = \Sigma_{l\epsilon\Omega}\,\phi_1\omega_l$. The estimates of the parameters $\{\hat{\alpha}, \hat{\mu}, \hat{\sigma}^2\}$ do not necessarily minimize the $\chi^2$ cost function and provide a suboptimal solution in the least-squares sense. The noise difference is evaluated as the difference of the actual and modeled time-series.

## ANALYSIS OF FMRI TIME-SERIES

In this section, we demonstrate how knowledge of the HDMF facilitates the evaluation of significant activations in response to a sensory or cognitive experiment. Although the discussion is confined to the univariate multiple regression, it is applicable to other statistical tests used in fMRI analysis as well.

With our notation, Eq. (2) in discrete-time domain becomes:

$$y_i = \alpha \sum_{l=1}^{n} h_{i(i-l)}x_l + \epsilon_i \qquad i = 1, 2, \ldots, n \quad (15)$$

where $h_{ij} = (1/\sqrt{2\pi\sigma^2})e^{-(i-j-\mu)^2/2\sigma^2}$ and $\epsilon_i$ is the noise for the ith sample of the time-series. Using matrix notation, the above equation may be succinctly written as

$$y = \alpha Hx + \epsilon \quad (16)$$

where $H = \{h_{ij}\}_{nxn}$ is referred to as the *modulation matrix* and $\epsilon = (\epsilon_1, \epsilon_2, \ldots, \epsilon_n)^T$.

The above equation for a single stimulus condition may be extended to experiments where a number of stimuli are simultaneously involved, assuming that their effects in producing the time-series are linear. For an experiment with a *design matrix* $[x_1, x_2, \ldots x_q, x_{q+1}, \ldots, x_{q+p}]$, where $x_1, x_2, \ldots, x_q$ represent q stimulus conditions and $x_{q+1}, x_{q+2}, \ldots, x_{q+p}$ represent p dummies [Friston et al., 1995a], Eq. (16) can be written as a standard regression equation:

$$y = X\beta + \epsilon \quad (17)$$

where $X = [H_1x_1, H_2x_2, \ldots, H_qx_q, x_{q+1}, \ldots, x_{q+p}]$ represents the set of hemodynamically modulated sensory stimuli, and $\beta = (\beta_1, \beta_2, \ldots, \beta_{q+p})^T$ represents the regression coefficients relating each stimulus condition to the time-series. $H_k$ denotes the modulation matrix for the kth stimulus condition $x_k$. Note that the dummy covariates were not modulated in the modified design matrix and that the gain of the model for each stimulus is now represented by the regression coefficients.

In order to find the values of regression coefficients, it is not possible to use inverse matrices for demodulation because of their ill-conditioned nature and sensitivity to the choice of HDMF. Therefore, a different approach is taken here by modulating only the stimulus condition $x_k$ when evaluating for the effect of the kth stimulus and finding the significance of the particular regression coefficient in predicting the time-series data, i.e., in order to check the effect of the stimulus condition $x_k$, Eq. (17) is written as

$$y = X_k\beta + \epsilon \quad (18)$$

where $X_k = [x_1 \ldots x_{k-1}\, H_kx_k x_{k+1} \ldots x_{p+q}]$ and $k \leq q$. In other words, the stimulation condition $x_k$ is subjected to the same modulation as experienced by the time-series, which is referred to as the *hemodynamic correction* of the time-series. Here the hemodynamic correction implies shifting of the input stimulus by a value equal to the lag and subjecting to temporal smoothing with a scale given by the square root of dispersion. Using Eq. (18), the significance of each condition in the design matrix in producing the time-series y is evaluated.

To test a single $\beta_k$ for significance or the hypothesis $H_0$: $\beta_k = 0$, we arrange $\beta_k$ last in $\beta$ such that $\beta = (\beta_k, \beta_k)$ and consider a reduced model without the condition $x_k$, i.e.,

$$y = X_k^*\beta_k + \epsilon_k \quad (19)$$

where $X_k^* = [x_1 \ldots x_{k-1}\, x_{k+1} \ldots x_{p+q}]$ is the design matrix and $\epsilon_k$ is the noise vector for the reduced model. The following *F*-statistic measures the significance of the kth stimulus condition of producing y [Rencher, 1995]:

$$F_k = d_k \frac{(\hat{\beta}^T X_k^T y - \hat{\beta}_k^T X_k^{*T} y)}{(y^T y - \hat{\beta}^T X_k^T y)} \quad (20)$$

where $d_k$ denotes degrees of freedom and $\hat{\beta} = (X_k^T X_k)^{-1} \cdot X_k^T y$ is the least-square estimate of the regression coefficients of the complete model. The estimate for the reduced model $\hat{\beta}_k$ is similarly obtained.

The data vector y in Eq. (17) represents a time-series which is smooth or autocorrelated in time, violating a major assumption of independence among data samples in regression analysis. The effective degrees of freedom associated with the correlated data are smaller than those associated with uncorrelated data, and the presence of autocorrelations increases the probability of spurious or high correlation coefficients by chance. The correlations among data points are compensated for by adjusting the degrees of freedom of the data. We use an approximate result for the effective degrees of freedom derived considering the error terms in the frequency-domain [Friston et al., 1995b]. If g is the error between the actual and estimated values of the time-series, then

$$g = y - X_k \hat{\beta}. \tag{21}$$

If $G(\omega_i)$ is the spectral density of the process g obtained using a discrete Fourier transform when $\omega_i = 2\pi i / (n - \text{rank}(X_k))$, the approximate value for the effective degrees of freedom $d_k$ is given by

$$d_k = \frac{(\Sigma_i G(\omega_i))^2}{\Sigma_i G^2(\omega_i)}. \tag{22}$$

Using Eq. (20), an *F*-statistical score indicating the significance of a stimulus in predicting the time-series is computed. An fMRI image consists of a set of time-series taken at contiguous spatial sites. If $y_j$ represents the time-series at the jth spatial location or voxel site, the fMRI image is given by the matrix $Y = [y_1, y_2, \ldots, y_m]$ where m denotes the total number of voxel sites. By following the above analysis, for each time-series $y_j$ and stimulus condition $x_k$, an *F*-statistical score $F_{jk}$ may be computed. The set $f_k = \{F_{k1}, F_{k2} \ldots F_{km}\}$ represents an *F*-statistical map for the kth stimulus condition, and is obtained using all the time-series in the fMRI image.

Defining a threshold for the statistical map to detect significant activations at a given probability level or *P*-value is not straightforward, because corrections for multiple independent statistical comparisons, and adjustments for spatial correlations due to correlated neural activities, need to be made. Because the activations appear as contiguous groups of image elements or make clusters of activated sites, this threshold has been related to the size of the activated regions. The minimum size of the regions of significant activations above a given threshold for z-statistical maps has been derived using the theory of Gaussian random fields [Friston et al., 1994a]. *F*-statistical maps obtained in the analysis are transformed to z-statistical maps using the transformation $\Phi(F) = \Psi(z)$ where $\Phi(\cdot)$ is the *F*-distribution function and $\Psi(\cdot)$ is the cumulative standard Gaussian function. With an experimentally determined threshold and a predetermined *P*-value, significantly activated regions from z-statistical maps for each stimulus condition are obtained. Subsequently, the significant activations are color-coded and registered onto the corresponding anatomical scans for display. The routines for processing fMRI images using the techniques described in this section were written in C++ and incorporated to the BRIAN image analysis system [Kruggel and Lohmann, 1996].

## EXPERIMENTS AND RESULTS

FMR images presented in this section were obtained on a 3.0 Tesla Medspec 30/100 scanner (Bruker Medizintechnik GmbH, Ettlingen, Germany) at the MRI Center of the Max-Planck-Institute of Cognitive Neuroscience. Images were obtained in visual-stimulation and word-recognition experiments using a FLASH protocol, and sentence-processing experiments were performed with an echo-planar imaging (EPI) protocol. All experiments were performed by German-speaking normal volunteers between age 20–30 years. The particular experiments were selected because of their pertinence to the ongoing research at the institute. In FLASH experiments, each slice was obtained separately by repeated application of the stimulation, while all the slices in the EPI experiments were obtained during a single presentation of the stimulation.

### Experiments with FLASH protocols

While a subject was performing the experiment, 3–6 two-dimensional $T_2^*$-weighted images, each with 64 scans, were acquired using a gradient-echo FLASH sequence (TR = 80.5 msec; TE = 40 msec; matrix = 128 × 64; The image matrices were zero-filled to obtain 128 × 128 images with a spatial resolution of 1.953 × 1.953 mm; slice thickness = 5-mm and 2-mm gap). The corresponding two-dimensional anatomical slices were also acquired with a $T_1$-weighted IR RARE sequence (TI = 900 msec; TR = 40 msec; TE = 3,900 msec; matrix = 512 × 512) in the same experiment session. In all experiments, ON and OFF stimuli were presented at a rate of 5.162 sec/sample. Each stimulation period had four successive stimulation ON states followed by four stimulation OFF states. The stimula-

**TABLE I. Characteristics of largest activated region on a selected slice in a visual-stimulation experiment obtained without hemodynamic correction (regression) and with hemodynamic correction using Poisson, Gamma, and Gaussian HDMFs***

| Model | Regression | Poisson | Gamma | Gaussian |
|---|---|---|---|---|
| Location | (68, 92) | (67, 93) | (67, 93) | (67, 94) |
| Size | 48.00 | 44.00 | 39.00 | 43.00 |
| z-score | 3.46 | 4.45 | 4.34 | 5.00 |
| Gain | 0.03 | 0.05 | 0.05 | 0.05 |
| Lag (s) | | 3.35 | 3.18 | 4.50 |
| Dispersion ($s^2$) | | 3.35 | 20.87 | 4.72 |
| Square error | 0.05 | 0.05 | 0.06 | 0.05 |
| $(S/N)_{z\text{-map}}$ (dB) | 16.68 | 18.23 | 17.92 | 19.53 |

* Location is given relative to the left topmost point of the image, size is given as number of voxels, and square error is the sum of the square error computed between the actual time-series and the fitted time courses by the model.

tions were repeated for eight cycles (total experiment time = 5.5 min), and experiments were carried out at different sessions with different subjects.

### *Visual-stimulation task*

An 8-Hz alternating checkerboard pattern with a central fixation point was projected on a LCD system, and subjects were asked to fixate on the point during stimulations. Images were acquired at three axial levels of the brain at the visual cortex.

### *Word-discrimination task*

During the stimulation period, subjects heard a random series of words and pronounceable nonwords (1.5 words per sec, 1:6 nonwords vs. words). Subjects were asked to count the nonwords per stimulation period (generally 6–7). Images at three sagittal levels were taken through the center of the temporal lobe on each side.

## Experiments with EPI protocols

Four $T_2^*$-weighted axial images (image matrix $128 \times 64$; slice thickness = 5 mm; gap = 2 mm; echo time TE = 40 msec; TR = 2.0 sec; flip angle = 40°) were acquired using a gradient echo, EPI protocol. The corresponding anatomical images were acquired as in FLASH experiments in the same session. Each stimulus period had three successive stimulus ON states and nine stimulus OFF states during stimulation presentation at 2 sec sample. An 18 sec intertrial interval completed a 24-sec run, for a total of 76 runs.

### *Sentence-processing task*

Single sentences which were correct or syntactically violated were binaurally presented to the subjects in a pseudorandomized order. Subjects were requested to respond by pressing a left button for a correct or a right button for an incorrect sentence.

## Data processing

The fMRI scans were corrected for possible subject movements by estimating the movement parameters by comparing each scan in the fMR image to a reference scan and realigning the scans using the parameters [Friston et al., 1996]. Movement-corrected images were filtered using a Gaussian filter with a standard deviation of 1 pixel and a spatial extent of 7 pixels in diameter (i.e., FWHM of 4.47 mm). The filtered images were analyzed using univariate multiple regression with hemodynamic correction, assuming a stimulation-dependent and space-variant Gaussian HDMF. The drift in the image intensities of the scans was considered as a linear dummy covariate. Significant activations were detected by thresholding the z-statistical maps and testing for significant regions at $P = 0.05$. The detected activities for each stimulus were mapped onto the corresponding anatomical slice for visual display. For EPI protocols, the lag values were corrected for the time delays between the stimulus presentation and the actual scanning of the slices [Van de Moortele et al., 1997], which were 0.52 sec, 1.11 sec, 0.67 sec, and 1.26 sec from the first to the fourth slice, respectively.

## Comparison of different HDMFs

Twenty FLASH data sets in our database were analyzed without making any adjustment for the lag and dispersion of the hemodynamic responses. Then they were analyzed after applying the hemodynamic correction separately with Poisson, Gamma, and Gaussian HDMFs. The parameters of the Poisson model were obtained using the modified-FJT method [Sorensen and Wang, 1997], and the parameters of the Gamma model were obtained by $\chi^2$-fitting using the Levenberg-Marquardt method [Press et al., 1994]. The one-pass algorithm presented above was used to determine the Gaussian model parameters.

For all the data sets compared, the adjustments for hemodynamic response resulted in visually better activations in the predicted areas of the brain with less spurious noise. The detected significant activations of a representative slice in a visual-stimulation experiment are shown in Figure 2, which is color-coded

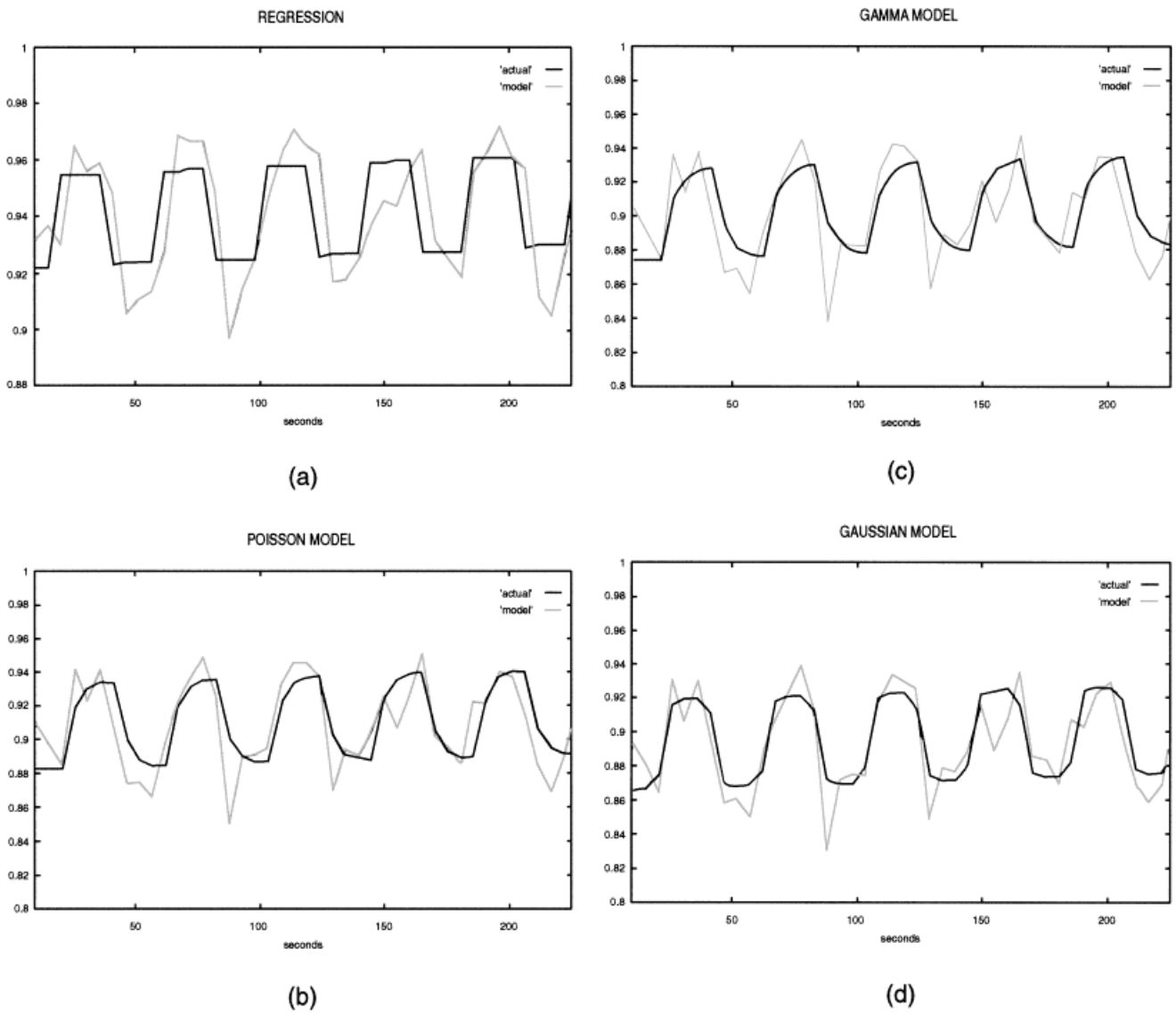


**Figure 3.**

Model fits obtained from time-series for the largest activation region in a visual-stimulation experiment using FLASH protocol at a sampling rate of 5.126 sec sample. **a:** Without hemodynamic correction. **b–d:** With hemodynamic correction, using (**b**) Poisson, (**c**) Gamma, and (**d**) Gaussian models.

according to the z-statistic. Significant activations were detected by thresholding z-maps at a threshold of 3.0 for regression analysis without hemodynamic correction, and 3.5 for the hemodynamically corrected analysis. Note that the hemodynamic correction reflected an increase in the average z-scores of the activated regions without generating spurious activities. The characteristics obtained by averaging over all the voxels in the largest activated region are shown in Table I. To compare the improvement of z-maps with the introduction of hemodynamic correction, the S / N ratio for the z-maps in dB is defined as follows:

$$(S/N)_{z\text{-map}} = 10 \log \left\{ \frac{z^2_{noise}}{z^2_{activations}} \right\} \qquad (23)$$

where $z^2_{noise}$ is the variance of the z-statistics of the nonactivated voxels, which is presumed to be superimposed on the average z-score of the activated voxels $z_{activations}$. Theoretically, the hemodynamic correction increases the z-scores of the activated voxels, but its

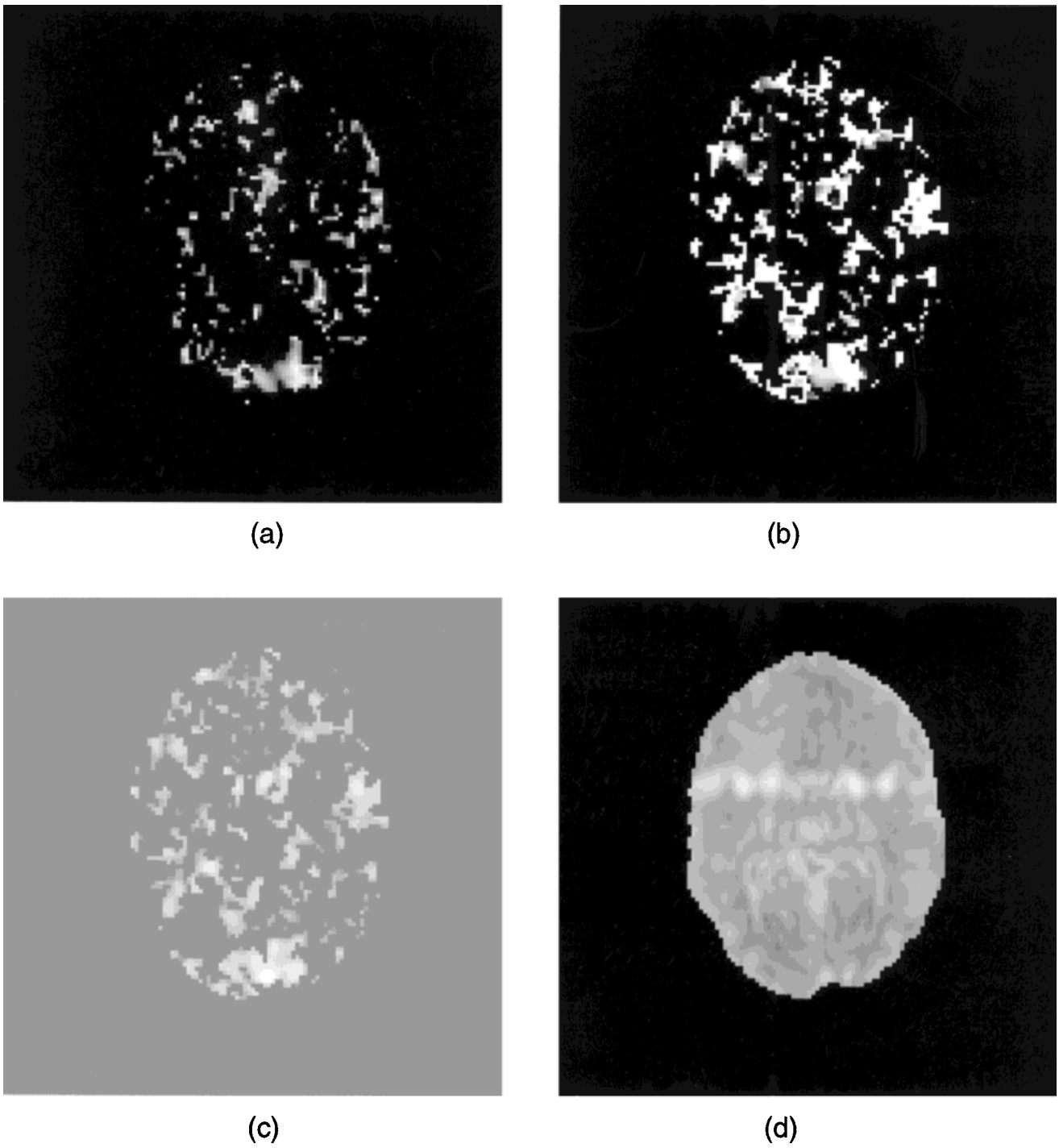


**Figure 4.**
Parameter maps computed over a representative slice obtained during a visual-stimulation experiment. Maps of (**a**) gain, (**b**) lag, (**c**) dispersion, and (**d**) noise where the intensity at a voxel represents values of the parameters.

**TABLE II. Comparison of hemodynamic parameters of the largest activated region and nonactivated region in a visual-stimulation experiment, using the t-test***

| | Gain | | Lag (s) | | Dispersion ($s^2$) | | Noise | |
|---|---|---|---|---|---|---|---|---|
| Region | Mean | SD | Mean | SD | Mean | SD | Mean | SD |
| Activated region | 0.053 | 0.024 | 4.504 | 0.915 | 4.721 | 2.628 | 0.050 | 0.032 |
| Nonactivated region | 0.000 | 0.004 | 0.577 | 2.308 | 0.471 | 2.356 | 0.013 | 0.031 |
| Significance (*P*-value) | $P < 0.001$ | | $P < 0.001$ | | $P < 0.001$ | | $P = 0.169$ | |

* Significance of the comarison in the tests is given as *P*-values.

effectiveness depends on its ability to avoid false alarms in the correction process. Hence, the above S / N ratio gives a quantitative measure for the improvement achieved in the hemodynamic correction.

Figure 3 shows the fMRI time courses obtained by averaging the time-series over the voxels of the largest activation blob and the fitted model waveforms using each HDMF. Note the drift in our data, which was corrected by using a linear dummy variable in the regression analysis. The actual time courses seen in the plots for the different models are different because the sizes of the detected regions slightly differ in some cases. Poisson and Gamma functions gave similar fits, while Gaussian functions gave a symmetrical fit at the rise and fall of stimulations.

Maps of gain, lag, dispersion, and noise values obtained in the particular slice in the visual-stimulation experiment are shown in Figure 4, where the intensities of the voxels represent the values of each parameter. The parameters of the largest region and the nonactivated voxels with their standard deviations are given in Table II. (The hemodynamic parameters for nonactivated voxels do not have any meaning, but result as a by-product of the analysis.) The differences of the hemodynamic parameters measured over the activated and nonactivated voxels were compared using t-tests. The significances or *P*-values of their differences of lag and dispersion at the two sites are also shown.

Data obtained in six EPI experiments were analyzed similarly as above, and improvements in the activity patterns were seen with hemodynamic correction for all data sets. The results of hemodynamic correction applied to all four slices of a representative experiment are shown in Figure 5. Note the improvement of the activations or z-maps with hemodynamic correction. Table III shows the characteristics of the largest activated region with and without hemodynamic correction and using multiple regression analysis for the third slice of the sequence.

### Space-dependence of hemodynamic parameters

In order to find the dependence of hemodynamic parameters on various brain sites during a sensory simulation, the images taken at six sagittal levels ($W_1 \ldots W_6$) in a representative word-discrimination experiment were analyzed. Figure 6 shows the detected activations of the corresponding slices with and without hemodynamic correction, assuming a Gaussian HDMF. The largest activation regions of six slices were compared among one another with t-tests for any discrepancies in lag and dispersion values. Significance of the differences or *P*-values is shown in Table IV. As seen in Table IV, the lag and dispersion values computed over some regions showed significant differences, while others were statistically similar.

### Intersubject variability of hemodynamic parameters

To investigate the intersubject variability of the hemodynamic parameters, three data sets ($V_1$, $V_2$, and $V_3$) at the same axial level, obtained while 3 different subjects separately performed the same visual-stimulation task, were analyzed. In all 3 cases, activations appear in the visual cortex, as seen in Figure 7, both with and without hemodynamic correction. The hemodynamic parameters of the largest activated regions of different subjects were compared using t-tests and their significances are shown in Table V. The lag values were significantly different between $V_1$ and $V_3$ and between $V_2$ and $V_3$, whereas the dispersions were statistically different between $V_1$ and $V_2$ and between $V_1$ and $V_3$.

## DISCUSSION

In the absence of proper understanding of the coupling between cerebral neuronal activity and associated hemodynamics, the linear convolution models

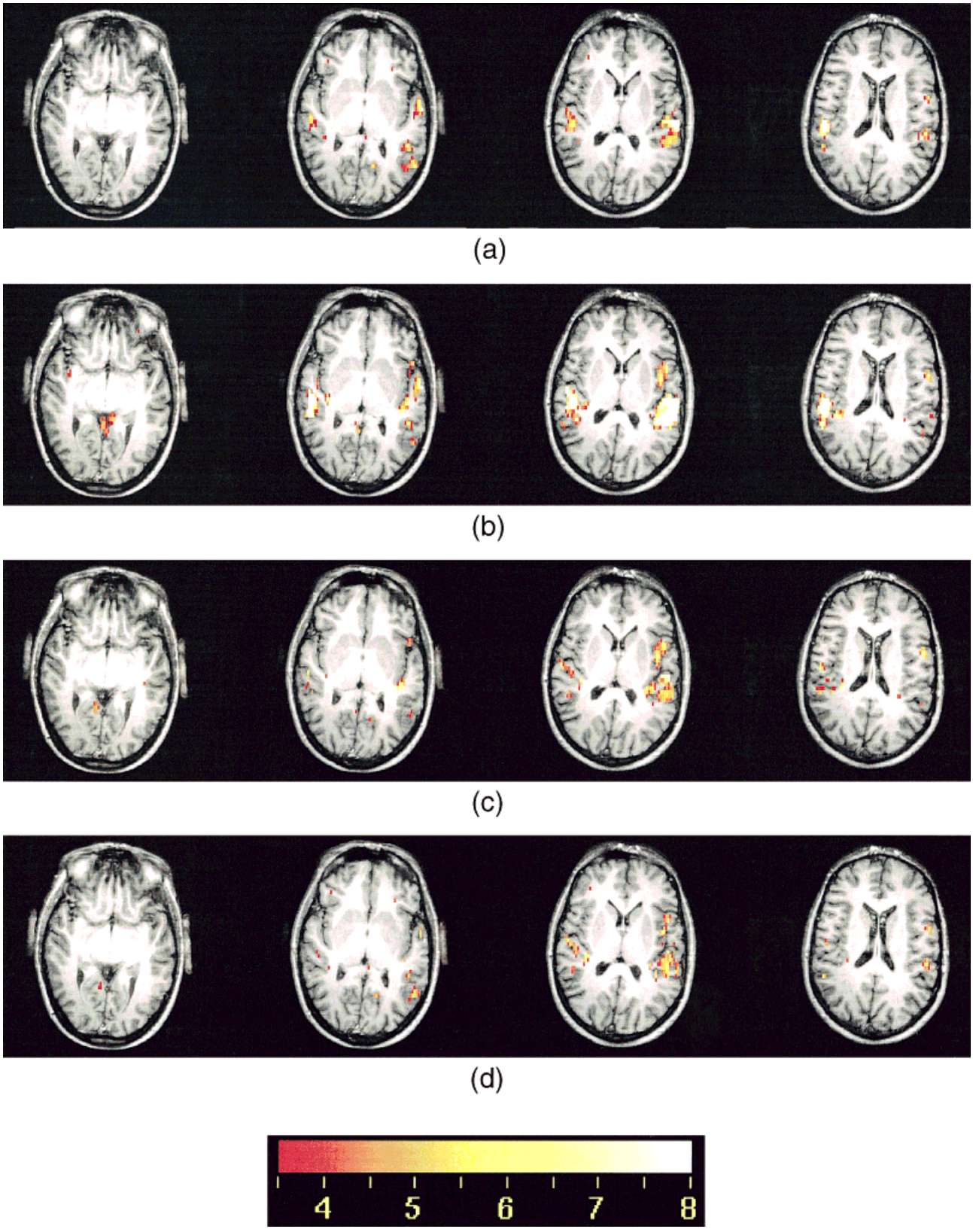


**Figure 5.**
Significant activations detected in a sentence-processing task imaged with an EPI protocol (sampling rate 2 sec/sample). Activities obtained (**a**) without hemodynamic correction ($z \geq 3.5$) and with hemodynamic correction ($z \geq 4.0$) using (**b**) Poisson, (**c**) Gamma, and (**d**) Gaussian models.

**TABLE III. Characteristics of largest activated region on a selected slice in a sentence-processing task obtained without hemodynamic correction (regression) and with hemodynamic correction using Poisson, Gamma, and Gaussian models***

| Slice no. | Regression | Poisson | Gamma | Gaussian |
|---|---|---|---|---|
| Location | (88, 38) | (87, 39) | (88, 39) | (87, 39) |
| Size | 58.00 | 88.00 | 45.00 | 41.00 |
| z-score | 5.72 | 7.38 | 5.51 | 5.80 |
| Gain | 0.01 | 0.21 | 0.01 | 0.01 |
| Lag (s) | | 20.65 | 0.05 | 3.81 |
| Dispersion ($s^2$) | | 20.65 | 0.27 | 1.58 |
| Square error | 0.27 | 0.33 | 0.28 | 0.27 |
| $(S/N)_{z\text{-map}}$ (dB) | 18.56 | 20.68 | 18.85 | 19.36 |

* Location is given relative to the left topmost point of the image, the size is given by the number of voxels, and the square error is the sum of error squares computed between the actual time-series and the fitted time course by the model.

present an approximate paradigm to study hemodynamic responses of human brain activation. The Gaussian HDMF presents a reasonable and flexible model to represent the delay and temporal correlations seen in fMRI time-series, and seems valid because the hemodynamic parameters determined in our experiments are closer to those previously reported [Frostig et al., 1990; Bandettini et al., 1993; Friston et al., 1994b]. Both Gamma and Poisson models are unable to account independently for the lag and dispersion of fMRI time-series because these parameters are linearly related. Our experiments with visual-stimulation, word-discrimination, and sentence-processing tasks demonstrated no clear relationship between the values of lag and dispersion of the hemodynamic responses of the activated regions. The two-parameter Gaussian model offers more flexibility and mathematical convenience to analyze hemodynamic responses in the brain than the previously proposed Poisson and Gamma models. However, the superiority of any model cannot be definitively concluded with our study, and comparison of different models is only possible with *chi-by-see* approach or by looking at the activities produced by different models in the same experiment.

The different models provide different temporal structures, and hence the values of hemodynamic parameters given by different models are different. A major disadvantage of the Gaussian function of HDMF is its symmetrical and infinite tails, precluding it from modeling asymmetries seen in the hemodynamic response and its reliance on past hemodynamic activities. Unlike the Gaussian model, the Poisson and Gamma models achieve the shape of HDMF by compromising between lag and dispersion values. The shapes of the fitted time-series using Poisson and Gamma functions are similar, whereas the Gaussian provides symmetric patterns at the onset and offset of the stimulus presentation. However, the asymmetry seen at the onset and offset of stimuli may be attributed to the different rise- and fall-times of neuronal activations [Rajapakse and Kruggel, 1997]. In the present study, we do not address transient aspects such as rise-time, fall-time, undershoot, and overshoot present in the fMRI, because they are initiated at the neuronal level and then modulated with HDMF. Nevertheless, these events can alter the frequency responses of time-series. This is a major limitation of all linear convolution models of hemodynamic response. Our experience with parametric models suggests that the HDMF behaves more likely as a Gamma function for a brief stimulus and as a Gaussian function for a prolonged stimulus. This may be because the negative tail of the Gaussian function allows considerable error for brief stimuli. However, there is no evidence to support our conjecture.

An advantage of the frequency-domain analysis is its ability to account for the noise in both time- and frequency-domains. Because frequency responses are computed on an average time-series cycle, the random noise and other variations of intensity that appear over the duration of the experiment are compensated for. Because only the responses at the harmonics of the fundamental frequency of time-series are considered in parameter estimation, frequency of stimulations can be designed to discount the artifactual changes contributed by other physiological processes such as heartbeat or pulsations in the cerebro-spinal fluid. Further investigation of the effects of these events and the frequencies used in our experiments for the analysis need to be done. The mathematical expressions used in frequency-domain analysis assume continuous and infinite time-series, which is practically prohibitive because stimuli are presented at discrete times within a finite period of time. The finite duration of fMRI time-series reflects as a rippling effect, and the sampling reflects as an aliasing effect in the frequency spectra [Brigham, 1988], introducing errors into the parameter estimations. These errors may be reduced by using high sampling rates and longer time-series. Another disadvantage of frequency-domain analysis is that it is applicable only for periodic stimulations. Frequency-domain analysis renders hemodynamic parameters for a Gaussian HDMF in a noniterative manner while with the Gamma model, parameter estimation leads to iterative and nonlinear optimization schemes. For nonperiodic stimulations, the param-

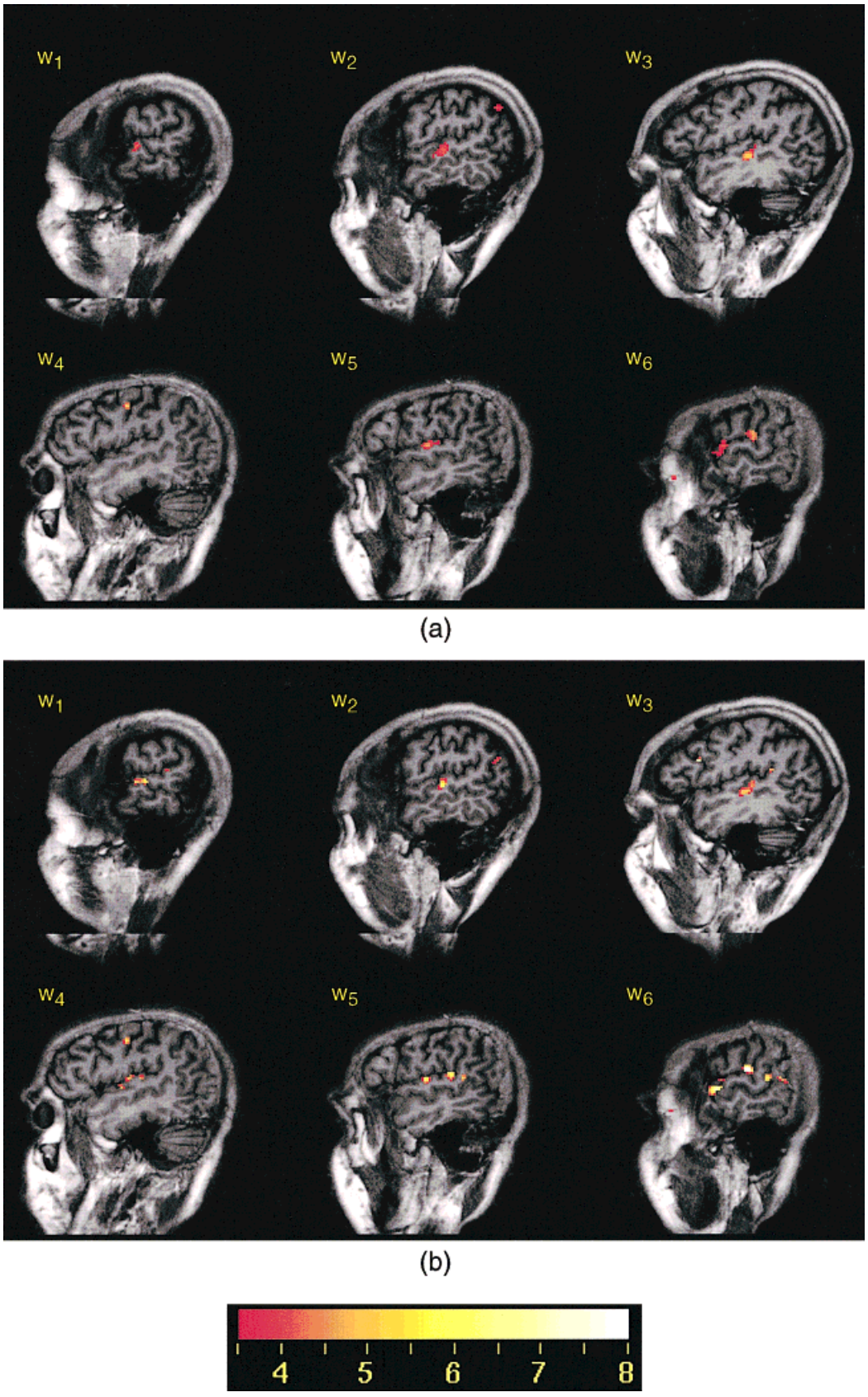


**Figure 6.**
Detected activities on six sagittal levels ($W_1 \ldots W_6$) of a representative subject performing a word-discriminating task. Using multiple regression (**a**) without hemodynamic correction ($z \geq 3.5$) and (**b**) with hemodynamic correction, assuming a Gaussian HDMF ($z \geq 4.0$).

**TABLE IV. Comparison of hemodynamic parameter-evaluated activities on six sagittal levels ($W_1 \ldots W_6$) on the same subject, assuming a Gaussian HDMF***

| | Lag | | | | | |
|---|---|---|---|---|---|---|
| | $W_1$ | $W_2$ | $W_3$ | $W_4$ | $W_5$ | $W_6$ |
| $W_1$ | 1.000 | 0.000 | 0.099 | 0.070 | 0.000 | 0.056 |
| $W_2$ | 0.000 | 1.000 | 0.000 | 0.068 | 0.000 | 0.000 |
| $W_3$ | 0.099 | 0.000 | 1.000 | 0.008 | 0.173 | 0.182 |
| $W_4$ | 0.070 | 0.068 | 0.008 | 1.000 | 0.000 | 0.000 |
| $W_5$ | 0.000 | 0.000 | 0.173 | 0.000 | 1.000 | 0.000 |
| $W_6$ | 0.056 | 0.000 | 0.182 | 0.000 | 0.000 | 1.000 |
| | Dispersion | | | | | |
| | $W_1$ | $W_2$ | $W_3$ | $W_4$ | $W_5$ | $W_6$ |
| $W_1$ | 1.000 | 0.026 | 0.806 | 0.000 | 0.004 | 0.853 |
| $W_2$ | 0.026 | 1.000 | 0.222 | 0.000 | 0.000 | 0.019 |
| $W_3$ | 0.806 | 0.222 | 1.000 | 0.000 | 0.055 | 0.744 |
| $W_4$ | 0.000 | 0.000 | 0.000 | 1.000 | 0.000 | 0.000 |
| $W_5$ | 0.004 | 0.000 | 0.055 | 0.000 | 1.000 | 0.005 |
| $W_6$ | 0.853 | 0.019 | 0.744 | 0.000 | 0.005 | 1.000 |

* Values indicated are the significance levels or *P*-values yielded in the comparison of the parameters of the two regions, using t-tests.

eters need to be computed for each cycle separately in frequency-domain or via piecewise model-fitting in the time-domain [Cohen, 1997], but both processes are computationally expensive.

The proposed Gaussian model with the parameter estimation scheme presented here facilitates the evaluation of hemodynamic responses at every voxel site. As demonstrated in our experiment, the concept of a global HDMF over the entire brain is incorrect. The hemodynamic response to neuronal activations is a complex function depending on the neuronal and vascular microarchitecture and the cognitive load in the region, and modulated by physiological factors such as pH, blood pressure, or metabolism. Because most of these factors may not be considered constant over the entire brain, we favored a space-variant approach. Our fMRI experiments resulted in different values of lag and dispersion for the activated regions for visual-stimulation and word-discrimination tasks, supporting our conjecture of a spatially-variant and stimulation-dependent hemodynamic response function for the brain. Although our experiments were not sufficient to make definitive conclusions about the nature of the variation of hemodynamic parameters, it became evident that they depended on a multitude of factors such as brain site, stimulus condition and frequency, or individual subject. Also, the comparison of functional activities based on the same experiment with different subjects is affected by the anatomical variability of the human brain, especially at the sulcal and gyral patterns, as seen in Figure 7. In other words, the functional variability is confounded by the anatomical variability of the human brain.

An exact formulation for the degrees of freedom was presented [Worsley and Friston, 1995] to compensate for the temporal correlations present in fMRI time-series. The idea of the smoothness matrix is not applicable when hemodynamics depend both on spatial location and on stimulation conditions. Therefore, the hemodynamic modulation needs to be applied to each stimulus separately. The threshold for the statistical maps to determine significant activation regions was determined empirically, considering all the data sets. There is no proper criterion for the selection of this threshold, although major developments were reported [Friston et al., 1994a] in this area with the theory of random Gaussian fields. Although smoothing in both time and space improves signal-to-noise ratios of the images, it might introduce artificial temporal or spatial correlations to the images and result in poor resolution of activation maps. In our approach, the spatial and temporal effects are handled separately, but a synergetic spatiotemporal approach may be more elegant and fruitful.

Univariate multiple regression analysis has been used earlier for statistical inference on significant activations with global hemodynamic parameters [Friston et al., 1995a], and an extension was presented to

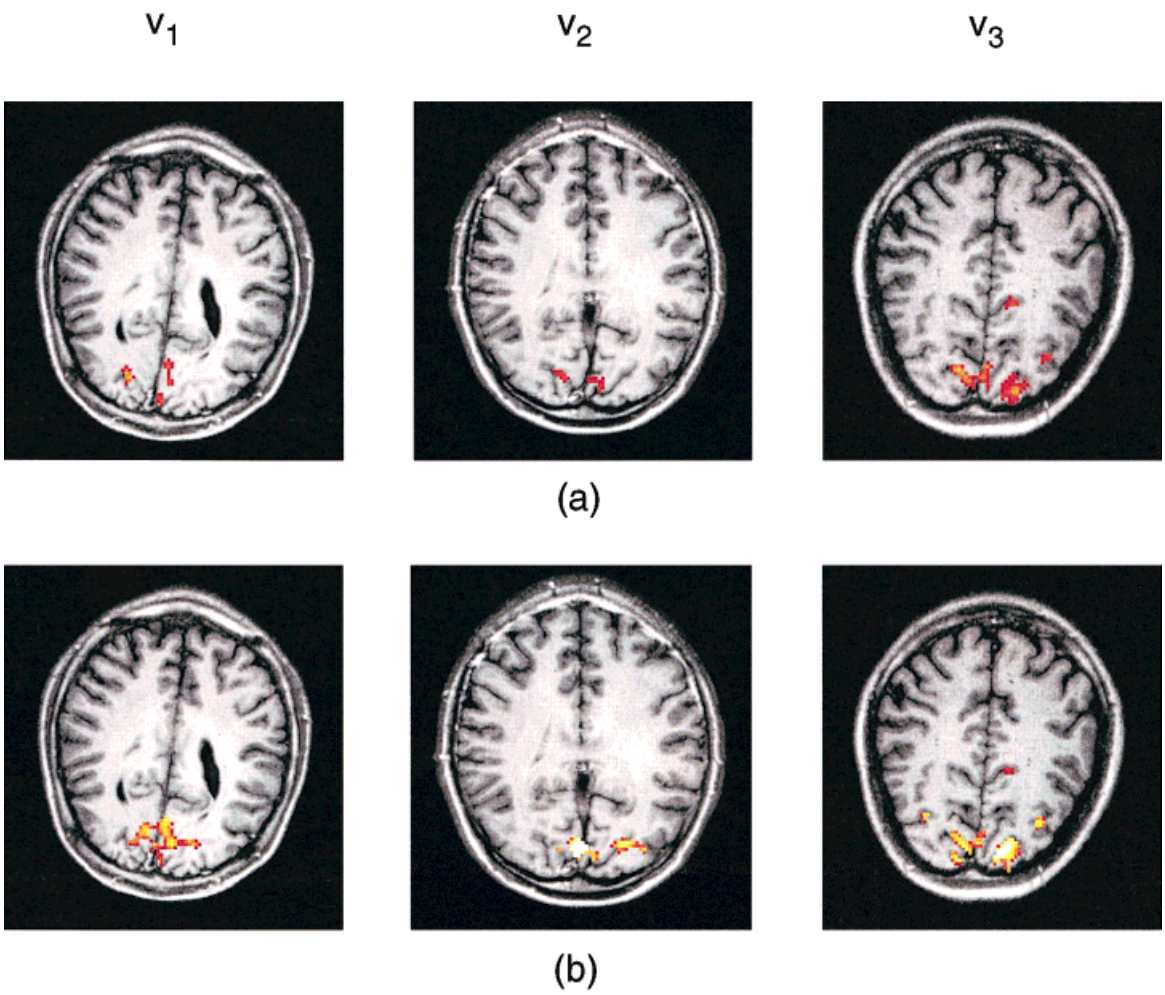


**Figure 7.**
Detected activities taken at the same axial level when 3 subjects ($V_1$, $V_2$, and $V_3$) separately performing the same visual-stimulation task (**a**) without hemodynamic correction ($z \geq 3.0$) and (**b**) with hemodynamic correction, using a Gaussian HDMF ($z \geq 3.5$).

**TABLE V. Comparison of hemodynamic parameters evaluated over the largest activated region at the same axial level on the different subjects ($V_1$, $V_2$, and $V_3$) separately performing the same visual task, assuming a Gaussian HDMF***

| | Lag | | | Dispersion | | |
|---|---|---|---|---|---|---|
| | $V_1$ | $V_2$ | $V_3$ | $V_1$ | $V_2$ | $V_3$ |
| $V_1$ | 1.000 | 0.824 | 0.001 | 1.000 | 0.009 | 0.003 |
| $V_2$ | 0.824 | 1.000 | 0.007 | 0.009 | 1.000 | 0.916 |
| $V_3$ | 0.001 | 0.007 | 1.000 | 0.003 | 0.916 | 1.000 |

* Values indicated are the significance levels or *P*-values obtained by comparing the parameters of the two regions, using t-tests.

handle locally varying hemodynamic parameters. Hemodynamic correction for lag and dispersion of fMRI time-series increased the sensitivity of our analysis, with an increase of the S/N ratio over the statistical maps. Incorporation of the hemodynamic correction for the statistical analysis is especially important when the frequency of the experimental stimulus is high with respect to the lag and dispersion values. Even though the experiments presented here had only a single stimulus condition, the analysis is applicable to experiments involving multiple stimuli and extendible in order to consider interactions among stimuli. Also, the methodology presented here is readily applicable to three-dimensional fMRI scans.

In deriving our simplified model, we neglected a number of important factors affecting the human brain

activation, e.g., the delay due to synaptic propagation of activity from sensory receptors to the brain voxels, the effect of ongoing activities over the brain, especially high level activities such as perception [Cerf et al., 1995] and their effect on experimental stimulus, and the nonlinearities posed by the MR scanners. Also, the psychological effects may not be significant in the tasks presented here, but may be significant in experiments involving multiple stimuli and higher cognitive tasks. The present model may be a basis for more complicated models to include other events that are assumed to be negligible in deriving our model. (For instance, our model may be extended adding another convolution term p(t) to account for the ''perception'' effect, which couples the neuronal activity extending Eq. (3): $y(t) = \alpha x(t) \otimes h(t) + \epsilon(t)$.) The subjects were presumed to have performed the experimental tasks identically over all the repeated presentations of the stimuli; nevertheless, the reaction times and behavior may well be different for each period. This violates our assumption of the stationarity of fMRI time-series and our deterministic approach. An extension to consider hemodynamic parameters as stochastic variables may be useful.

Physiologically, finite values of lag and dispersion for activated regions indicate that the change in blood-oxygenation takes time to respond to a change in neural firing at a slower pace than the changes of the stimulus condition. These parameters were different for activated and nonactivated sites and may be related to the structure, morphology, vasculature, and metabolism of the cortex and useful in characterizing and categorizing the activated sites. Further investigation of these parameters throughout the cortex may unravel salient aspects of its functional specificity. However, it is necessary to further validate the Gaussian and other models representing brain hemodynamics before making conclusions about brain functions. Until the process of vascular coupling of neuronal activations is well-understood and an accurate and well-parameterized model for functionally induced MR signal changes is established, our model may serve as a valuable tool for functional neuroimaging studies. It may be useful as a prototype for more complex models of HDMF to include other aspects of hemodynamic responses, such as transient and habituation effects during sensory or cognitive stimulation tasks.

## ACKNOWLEDGMENTS

We thank our colleagues Ulrich Müller, Stephan Pollmann, and Christian Uhl for their input into the manuscript. Experiments were conducted by Chris Wiggins, Margret Hund, and Thoralf Niendorf.

## REFERENCES

Bandettini PA, Jesmanowicz A, Wong EC, Hyde JS (1993): Processing strategies for time-course data sets in functional MRI of human brain. Magn Reson Med 30:161–173.

Bandettini PA, Wong EC, Jesmanowicz A, Hinks RS, Hyde JS (1994): Spin-echo and gradient-echo EPI of human brain activation using BOLD contrast: A comparative study at 1.5T. NMR Biomed 7:12–20.

Belliveau JW, Kennedy DN, McKinstry RC, Buchbinder BR, Weisskoff RM, Cohen MS, Vevea JM, Brady TJ, Rosen BR (1991): Functional mapping of the human cortex by magnetic resonance imaging. Science 254:716–719.

Blamire AM, Ogawa S, Ugurbil K, Rothman D, McCarthy G, Ellermann JM, Hyder F, Rattner Z, Shulman RG (1992): Dynamic mapping of the human visual cortex by high-speed magnetic resonance imaging. Proc Natl Acad Sci USA 89:11069–11073.

Brigham EO (1988): The Fast Fourier Transform and Its Applications, Englewood Cliffs: Prentice Hall.

Bullmore E, Brammer M, Williams SCR, Rabe-Hesketh S, Janot N, David A, Mellers J, Howard R, Sham P (1996): Statistical methods of estimation and inference for functional MR image analysis. Magn Reson Med 35:261–277.

Cerf B, Van de Moortele E, Giacomini E, MacLeod P, Faurion D, Le Bihan D (1996): Correlation of perception to temporal variations of fMRI signal: A taste study. Proceedings of the Fourth Meeting of the International Society for Magnetic Resonance in Medicine, Berkeley: International Society for Magnetic Resonance in Medicine, p. 477.

Cohen MS (1997): Parametric analysis of fMRI data using linear systems methods. Neuroimage 6:93–103.

Duyn JH, Moonen CTW, van Yperen GH, de Boer RW, Luyten PR (1994): Inflow versus deoxyhemoglobin effects in BOLD functional MRI using gradient echoes at 1.5T. NMR Biomed 7:83–88.

Engel SA, Rumelhart DE, Wandell BA, Lee AT, Glover GH, Chichilnisky E-J, Shadlen MN (1994): fMRI of human visual cortex. Nature 369:525.

Ernst T, Henning J (1994): Observation of fast response in functional MR. Magn Reson Med 32:146–149.

Fox PT, Raichle ME (1986): Focal physiological uncoupling of cerebral blood flow and oxidative metabolism during somatosensory stimulation in human subjects. Proc Natl Acad Sci USA 83:1140–1144.

Fox PT, Raichle ME, Mintun MA, Dence C (1988): Nonoxidative glucose consumption during focal physiologic neural activity. Science 241:462–464.

Frahm J, Merboldt K-D, Hanicke W, Kleinschmidt A, Boecker H (1994): Brain or vein—Oxygenation of flow? On signal physiology in functional MRI of human brain activation. NMR Biomed 7:45–53.

Friston KJ, Worsley KJ, Frackowiak RSJ, Mazziotta JC, Evans AC (1994a): Assessing the significance of focal activations using their spatial extent. Hum Brain Mapp 1:210–220.

Friston KJ, Jezzard P, Turner R (1994b): Analysis of functional MRI time-series. Hum Brain Mapp 1:153–171.

Friston KJ, Holmes AP, Worsley KJ, Poline JB, Frith CD, Frackowiak RSJ (1995a): Statistical parametric maps in functional imaging: A general linear approach. Hum Brain Mapp 2:189–210.

Friston KJ, Holmes AP, Poline J-B, Grasby PJ, Williams CR, Frackowiak SJ, Turner R (1995b): Analysis of fMRI time-series revisited. Neuroimage 2:45–53.

Friston KJ, Williams S, Howard R, Frackowiak RSJ, Turner R (1996): Movement-related effects in fMRI time-series. Magn Reson Med 35:346–355.

Frostig RD, Lieeke EE, Ts'o YD, Grinvald A (1990): Cortical functional architecture and local coupling between neuronal activity and the microcirculation revealed by *in vivo* high-resolution optical imaging of intrinsic signal. Proc Natl Acad Sci USA 87:6082–6086.

Jueptner M, Weiller C (1995): Review: Does measurement of regional cerebral blood flow reflect synaptic activity? Implications for PET and fMRI. Neuroimage 2:148–156.

Kruggel F, Lohmann G (1996): BRIAN—A toolkit for the analysis of multimodal brain data sets. In: Lemke HV, Inamura K, Jaffe CC, Vannier MW (eds): Proceedings of the Computer Assisted Radiology (CAR 96). Berlin: Springer-Verlag, pp 323–328.

Kwong KK, Belliveau JW, Chesler DA, Goldberg IE, Weisskoff RM, Poncelet BP, Kennedy DN, Hoppel BE, Cohen MS, Turner R, Cheng H-M, Brady TJ, Rosen BR (1992): Dynamic magnetic resonance imaging of human brain activity during primary sensory stimulation. Proc Natl Acad Sci USA 89:5675–5679.

Lange N, Zeger SL (1997): Non-linear Fourier time series analysis for human brain mapping by functional magnetic resonance imaging. J R Stat Soc Appl Stat 46:1–29.

Lee AT, Glover GH, Meyer GH (1995): Discrimination of large venous vessels in time-course spiral blood-oxygen-level-dependent magnetic resonance functional neuroimaging. Magn Reson Med 33:745–754.

Maisog JM, Clark V, Courtney S, Haxby J (1995): Estimating the hemodynamic response and effective degrees of freedom in functional MRI time series. First International Conference on Functional Mapping of the Human Brain Abstracts, Supplement 1, p 147.

McCarthy G, Blamire AM, Rothman DL, Gruetter R, Shulman RG (1993): Echo-planar magnetic resonance imaging studies of frontal cortex activation during word generation in humans. Proc Natl Acad Sci USA 90:4952–4956.

Menon RS, Ogawa S, Tank DW, Ugurbil K (1993): 4 Tesla gradient recalled echo characteristics of photic stimulation-induced signal changes in the human primary visual cortex. Magn Reson Med 30:380–386.

Menon RS, Ogawa S, Hu X, Strupp JP, Anderson P, Ugurbil K (1995): BOLD based functional MRI at 4 Tesla includes a capillary bet contribution: Echo-planar imaging correlates with previous optical imaging using intrinsic signals. Magn Reson Med 33: 453–459.

Nielsen FA, Hansen LK, Toft P, Goutte C, Lange N, Strother SC, Morch N, Svarer C, Savoy R, Rosen B, Rostrup E, Born P (1997): Comparison of two convolution models for fMRI time series. Toga A., Frachouide RSY, Mazzotta JC (Eds.) Third International Conference on Functional Mapping of the Human Brain, San Diego: Academic Press, p. 473.

Ogawa S, Tank DW, Menon R, Ellermann JM, Kim S-G, Merkle H, Ugurbil K (1992): Intrinsic signal changes accompanying sensory stimulation: Functional brain mapping with magnetic resonance imaging. Proc Natl Acad Sci USA 89:5951–5955.

Ogawa S, Menon RS, Tank DW, Kim S-G, Merkle H, Ellermann JM, Ugurbil K (1993): Functional brain mapping by blood oxygenation level-dependent contrast magnetic resonance imaging. Biophys J 64:803–812.

Papoulis A (1991): Probability, Random Variables, and Stochastic Processes, Third Edition, New York: McGraw-Hill, Inc.

Press WH, Teukolsky SA, Vetterling WT, Flamery BP (1994): Numerical Recipies in C, Cambridge: Cambridge University Press.

Raichle ME, Grubb RL, Gado MH, Eichling JO, Ter-Pogossian MM (1976): Correlation between regional cerebral blood flow and oxidative metabolism. Arch Neurol 33:523–526.

Rajapakse JC, Kruggel F (1997): Neuronal and hemodynamic responses from fMRI time-series. Proceedings of International Conference on Neural Information Processing, New Zealand.

Rencher AC (1995): Methods of Multivariate Analysis, New York: John Wiley & Sons, Inc., p 360.

Turner R, Jezzard P, Wen H, Kwong KK, Le Bihan D, Zeffiro T, Balaban RS (1993): Functional mapping of the human visual cortex at 4 and 1.5 Tesla using deoxygenation contrast EPI. Magn Reson Med 29:277–279.

Singh M, Kim T, Kim H, Khosla D (1995): Separation of veins from activated brain tissue in functional magnetic resonance images at 1.5T. IEEE Trans Nucl Sci 42:1338–1340.

Sorenson JA, Wang X (1997): Problems in estimating hemodynamic response parameters from fMRI data. Hum Brain Mapp 4: 265–272.

Van de Moortele PF, Lobel E, Paradis AL, Le Bihan D (1997): Brain activation analysis of EPI fMRI time series needs correction for slice dependent phase shifts. Proceedings of the Fifth Meeting of the International Society for Magnetic Resonance in Medicine, Berkeley: International Society for Magnetic Resonance in Medicine, p. 129.

Villringer A, Dirnagl U (1995): Coupling of brain activity and cerebral blood flow: Basis of functional neuroimaging. Cerebrovasc Brain Metab Rev 7:240–276.

Worsley KJ, Friston KJ (1995): Analysis of fMRI time-series revisited—again. Neuroimage 2:173–181.

## APPENDIX
### Parametric models for Hemodynamic Modulation Function (HDMF)

| Model | HDMF | Fourier transform | (Lag, dispersal) | Comments |
|---|---|---|---|---|
| Poisson | $P(i) = \lambda^i e^{-\lambda}/i!$ | | $(\lambda, \lambda)$ | $i \epsilon N^+$; $\lambda \epsilon R^+$<br>Lag = dispersion |
| Gamma | $\Gamma(t) = \theta_2^{\theta_1} t^{\theta_1 - 1} e^{-\theta_2 t}/\Gamma(\theta_1)$ | $(1 - jw_i/\theta_2)^{-\theta_1}$ | $\left(\frac{\theta_1}{\theta_2}, \frac{\theta_1}{\theta_2^2}\right)$ | $\theta_1, \theta_2 \epsilon R^+$<br>Lag = dispersion $\gamma_2$ |
| Gaussian | $G(t) = \frac{1}{\sqrt{2\pi\sigma^2}} e^{-(t-\mu)^2/\sigma^2}$ | $e^{-\omega^2\sigma^2/2} e^{-j\omega\mu}$ | $(\mu, \sigma^2)$ | $\mu \epsilon R$; $\sigma^2 \epsilon R^+$ |